

# 1 Homogenization of fault frictional properties

2 **Sohom Ray<sup>1</sup> and Robert C. Viesca<sup>1</sup>**

3 <sup>1</sup>Department of Civil and Environmental Engineering, Tufts University, Medford, MA, USA

## 4 **Key Points:**

- 5 • Analysis of non-linear instabilities elucidates role of heterogeneity in fault frictional  
6 properties.
- 7 • Properties homogenizable when parameters vary over distances smaller than elasto-  
8 frictional length.
- 9 • Non-trivial dynamics emerge when parameters vary over distances comparable to  
10 that length.

11      **Abstract**

12      The frictional properties of large faults are expected to vary in space. However, fault  
 13     models often assume properties are homogeneous, or nearly so. We investigate the con-  
 14     ditions under which the details of variations may be neglected and properties homog-  
 15     enized. We do so by examining the behavior of non-linear solutions for unstably accel-  
 16     erating fault slip under frictional heterogeneity. We consider a rate- and state-dependent  
 17     fault friction, in which the characteristic wavelength for the property variations is a prob-  
 18     lem parameter. We find that homogenization is permissible only when that wavelength  
 19     shows scale separation from an elasto-frictional length scale. However, fault models also  
 20     often include property transitions that occur over distances comparable to the elasto-  
 21     frictional length. We show that under such comparable variations, the dynamics of earthquake-  
 22     nucleating instabilities are controlled by the properties' spatial distribution.

23      **Plain language summary**

24      Faults have several potential sources of complexity, including their roughness as  
 25     well as the heterogeneity of fault strength, stress, and structure. How do these affect the  
 26     dynamics of fault slip in the seismic cycle, alone or together? Here we focus on under-  
 27     standing the effect of spatial variation of fault frictional properties. However, laboratory  
 28     experiments indicate that fault frictional strength is highly non-linear such that this av-  
 29     enue may not appear fruitful. Nonetheless, we find a means to make headway by apply-  
 30     ing recent developments in the understanding of how instabilities develop on model faults.  
 31     We examining behavior of instability solutions as properties vary under relatively long  
 32     or short distances. We find that faults whose frictional properties vary relatively rapidly  
 33     behave as if the properties are uniform, where only the average values are relevant. When  
 34     properties vary relatively moderately, the variations cannot be ignored and preferential  
 35     sites for nucleation can result, sometimes in unexpected places.

36      **1 Introduction**

37      Following laboratory rock friction studies (e.g., Stesky, 1975; Dieterich, 1981; Blan-  
 38     pied et al., 1991) fault frictional properties at depth have been thought to be vary with  
 39     depth and this variation has been reflected in seismic cycle models (e.g., Tse & Rice, 1986).  
 40     Often, simple representations of these variations on mature faults are chosen: homogene-  
 41     ity over large intervals with transitions occurring further down dip. However, several ob-

42 servations indicate that frictional heterogeneity may exist over large regions of a fault  
43 at various scales, observations such as the clustering of microseismicity (e.g., Rubin &  
44 Ampuero, 2005; Waldhauser et al., 2004). This raises questions as to what extent can  
45 homogeneity be taken in place of considering detailed distribution of properties. Specif-  
46 ically, is it possible to lose important information by using averages of variable quanti-  
47 ties. In other words, can homogenizing be ingenuous? How does the presence or absence  
48 of homogeneity affect the dynamics of models of seismic cycles?

49 Past studies of the influence of heterogeneity on fault rupture have focused on rate-  
50 independent descriptions of fault strength, as implied by a slip-dependent strength or  
51 the assumption of a constant fracture energy. Such descriptions lend themselves to ap-  
52 plication of concepts from classical, linear-elastic fracture mechanics, in which knowledge  
53 of the spatial distribution of stress or strength is used to make predictions regarding rup-  
54 ture propagation and arrest. For example, fault stress may be presumed to vary in space,  
55 while properties determining frictional strength are taken to be uniform, such as in the  
56 determination of rupture extent in numerical simulations or in experimental, laboratory  
57 ruptures Ampuero et al. (2006); Ripperger et al. (2007); Kammer et al. (2015); Bayart  
58 et al. (2015); Ke et al. (2018). In the former, the stress field is known such that rupture  
59 extent can be predicted a priori, and in the latter rupture extent is predicted retrospec-  
60 tively using measurements of stress changes following rupture. While in both examples,  
61 the so-called fracture energy of the fault is typically presumed a material constant, there  
62 has also been an interest in understanding how variations of the fault fracture energy,  
63 by way of varying frictional properties, affect the statistics of rupture events (e.g., Aochi  
64 & Ide, 2004).

65 However, laboratory and theoretical studies indicate that fault strength has a rate-  
66 dependence, in manners such that the fracture energy may not be considered to be a lo-  
67 cal property of the fault. The dependence may be weak at interseismic slip rates (Ru-  
68 ina, 1983, e.g.) or strong for mechanisms thought to operate during fast, co-seismic slip  
69 (e.g., Rice, 2006; Goldsby & Tullis, 2011). This rate dependence, however, raises diffi-  
70 culties in the analysis of spatial variations of frictional properties. Here we focus on the  
71 problem of earthquake nucleation to begin to address the above questions. Specifically,  
72 we consider a slip rate- and state-dependent fault friction and we examine instability de-  
73 velopment on faults with spatial distributions of frictional parameters. Prior work has  
74 considered the emergence of earthquake-nucleating instabilities on faults with spatially

75 uniform properties using both linear Rice & Ruina (1983); Rice et al. (2001); Aldam et  
 76 al. (2017) and non-linear Dieterich (1992); Rubin & Ampuero (2005); Viesca (2016a,b)  
 77 analysis and numerical solutions. Using recent developments for the analysis of insta-  
 78 bility under heterogeneous frictional properties Dublanchet (2017); Ray & Viesca (2017),  
 79 we seek to determine the role of the length scale over which properties transition.

## 80 2 Equations governing quasi-static fault slip

### 81 2.1 Fault shear traction

82 We consider a geological fault as an interface, within a continuum, that accommo-  
 83 dates relative motion. The fault is presumed to be located along  $x - z$  plane contain-  
 84 ing the origin; and we consider in- or anti-plane deformation in which the magnitude of  
 85 the displacement varies only over  $x$ . The ambient stress and displacement fields in the  
 86 medium are identified respectively as  $\sigma_{ij}(x, y, t)$  and  $u_i(x, y, t)$ . On the fault, the mag-  
 87 nitude of the displacement discontinuity is referred to as slip, which is considered to vary  
 88 only along  $x$  and is given by  $\delta(x, t) = u_i(x, 0^+, t) - u_i(x, 0^-, t)$ , where  $i = x$  or  $z$  de-  
 89 note in-plane (mode II) or anti-plane (mode III) shearing respectively.

90 In absence of any differential slip along the fault, the shear traction on the fault  
 91 surface is purely due to any remote loading, which resolves onto the fault surface as  $\tau_{ex}$ .  
 92 When the fault accommodates slip, the fault shear traction changes by an amount  $\tau_{el}$ ,  
 93 due to the elastic deformation of the fault bounding medium. The total fault shear trac-  
 94 tion  $\tau$  due to the medium's loading and response to nonuniform slip is then, given by,

$$95 \quad 96 \quad \tau(x, t) = \tau_{ex}(x, t) + \tau_{el}(x, t) \quad (1)$$

97 We consider here slow, quasistatic deformation in which  $\tau_{el}$  is determined by the  
 98 current distribution of the slip  $\delta(x, t)$ . For in- or anti-plane slip on an unbounded fault  
 99 between two elastic half spaces

$$100 \quad 101 \quad \tau_{el}(x, t) = \frac{\bar{\mu}}{2\pi} \int_{-\infty}^{\infty} \frac{\partial \delta(\xi, t)/\partial \xi}{\xi - x} d\xi \quad (2)$$

102 where  $\bar{\mu} = \mu/(1 - \nu)$  and  $\bar{\mu} = \mu$  for in- and anti-plane slip, respectively (e.g., Bilby &  
 103 Eshelby, 1968; Rice, 1968). For a fault lying below and parallel to a free surface a dis-  
 104 tance  $h$  away,  $\tau_{el}$  is more simply expressed as

$$105 \quad 106 \quad \tau_{el}(x, t) = \bar{E}h \frac{\partial^2 \delta(x, t)}{\partial x^2} \quad (3)$$

provided that variations in slip  $\delta(x, t)$  occur over distances much larger than  $h$  [supplementary materials, Viesca (2016a)], where the elastic modulus  $\bar{E} = 2\mu/(1-\nu)$  and  $\bar{E} = \mu$  for mode-II and mode-III sliding respectively.  $\mu$  and  $\nu$  are the shear modulus and Poisson's ratio, respectively.

Such a so-called thin slab configuration has been presumed to well represent the elastic deformation of translational landslides and ice sheets in response to basal slip (e.g., Puzrin & Germanovich, 2005; Lipovsky & Dunham, 2017), and also as a more mathematically convenient representation of elastic interactions between points on a fault (e.g., Bar-Sinai et al., 2012). As discussed in Viesca (2016a,b) and Ray & Viesca (2017), the two models, while representing two end-members of elastic interactions, long- and short-ranged, can give rise to qualitatively similar behavior. In the sections to follow, we present results for the thin-slab fault-model, though the results are generally qualitatively similar to the elastic configuration.

## 2.2 Fault frictional strength

We presume the fault shear strength,  $\tau_s$ , is purely frictional and given by

$$\tau_s(x, t) = \sigma(x, t)f(x, t) \quad (4)$$

where  $\sigma$  is the fault-normal stress and  $f$  is the friction coefficient. In the case of a fluid-saturated fault zone,  $\sigma$  is the effective fault-normal stress,  $\sigma(x, t) = \sigma_n(x, t) - p(x, t)$ , where  $\sigma_n(x, t)$  is the total normal stress and  $p(x, t)$  is the pore fluid pressure. We consider a rate- and state-dependent formulation Dieterich (1978); Ruina (1983) in which  $f$  is a function of the instantaneous rate of slip  $V(x, t) = \partial\delta/\partial t$ , a state variable  $\theta(x, t)$ , and heterogeneous material parameters  $a(x)$  and  $b(x)$  at that position

$$f(x, t) = f_o + a(x) \ln \left[ \frac{V(x, t)}{V_o} \right] + b(x) \ln \left[ \frac{\theta(x, t)}{\theta_o} \right] \quad (5)$$

We consider, the aging-law evolution of state Ruina (1983), in which,

$$\frac{\partial\theta}{\partial t} = 1 - \frac{V(x, t)\theta(x, t)}{D_c(x)}. \quad (6)$$

Here,  $D_c(x)$  is the characteristic slip over which friction evolves which we also allow to vary along the fault. The formulation exhibits the logarithmic rate dependence for steady-state sliding ( $\partial\theta/\partial t = 0$ ) as shown below.

$$f_{ss}(x, t) = f_o + [a(x) - b(x)] \ln \left[ \frac{V(x, t)}{V_o} \right]$$

140 In (5) and above,  $f_o$  is the reference coefficient of friction at steady sliding veloc-  
 141 ity  $v_o$  and state  $\theta_o = D_c/V_o$ . Fault surfaces with  $a < b$  are potentially destabilizing  
 142 because an increase in sliding rate subsequently leads to a weakened new steady-state  
 143 shear strength. Such steady-state rate-weakening surfaces, when subjected to stress or  
 144 velocity perturbations can lead to an instability that might nucleate an earthquake gen-  
 145 erating dynamic rupture (e.g., Rice & Ruina, 1983)

146 Considering the form of slip acceleration (Supplementary Materials) motivates us  
 147 to choose an alternate state variable  $\Phi(x, t)$  given by

$$148 \quad 149 \quad \Phi(x, t) = -\frac{D_c(x)}{V(x, t)} \frac{\partial \theta / \partial t}{\theta(x, t)} \quad (7)$$

150 which for the aging law of state evolution assumes the form

$$151 \quad 152 \quad \Phi(x, t) = 1 - \frac{D_c(x)}{V(x, t)\theta(x, t)}. \quad (8)$$

153 With this definition,  $\Phi(x, t)$  can be interpreted as a convenient measure for nearness of  
 154 fault slip to steady-state sliding:  $\Phi = 0$  occurs for steady state sliding and  $\Phi = 1$  when  
 155 the state of the slip is far from steady state.

### 156 2.3 Slip rate and state evolution equations

157 Frictional resistance requires that when and where slip rate is nonzero the total shear  
 158 stress is equal to the strength of the fault  $\tau(x, t) = \tau_s(x, t)$ . Evolution equations for slip  
 159 rate and the alternate state variable  $\Phi$  follow from the equations in Section 2 and are  
 160 expressible in the form

$$161 \quad \frac{\partial V}{\partial t} = \mathcal{R}[V(x, t), \Phi(x, t)] \quad (9a)$$

$$162 \quad 163 \quad \frac{\partial \Phi}{\partial t} = \mathcal{S}[V(x, t), \Phi(x, t)] \quad (9b)$$

164 where the operators  $\mathcal{R}$  and  $\mathcal{S}$  depend on the elastic configuration, the distribution of  $a(x)$ ,  
 165  $b(x)$  and  $D_c(x)$ , and also on the external stress-rate [Supplementary Materials], though  
 166 we have dropped explicit reference to these latter terms here.

167 The interaction between the elasticity of the bounding medium and the frictional  
 168 strength of the interface defines an elasto-frictional length scale for strength and slip vari-  
 169 ations along the interface. For an interface lying within a full-space, such a length scale  
 170 is  $L_b = \bar{\mu}D_c/b\sigma$  Dieterich (1992); Rubin & Ampuero (2005), when the evolution-effect  
 171 parameter  $b$  is uniform. Likewise, for the thin-slab configurations, a length scale is  $L_{bh} =$

<sup>172</sup>  $\sqrt{EhD_c/b\sigma}$  Viesca (2016a,b). When  $a$  or  $b$  vary, we may use instead  $L_n = \bar{\mu}D_c/\sigma$  and  
<sup>173</sup>  $L_{nh} = \sqrt{\bar{E}hD_c/\sigma}$ , for the and thin-slab configurations, respectively Ray & Viesca (2017).

### <sup>174</sup> 3 Finite-time instability of slip rate

<sup>175</sup> Prior work showed the existence of solutions in which slip rate quasi-statically di-  
<sup>176</sup> verges within finite time on faults with heterogeneous frictional parameters Ray & Vi-  
<sup>177</sup> esca (2017). Specifically, the solutions have the form

$$\text{<sup>178</sup> } V(x, t) = \frac{D_c(x)}{t_f(t)} \mathcal{W}(x) \quad (10)$$

<sup>180</sup> where  $t_f(t) = t_{in} - t$ ,  $t_{in}$  is the finite time of the instability, and the spatial distribu-  
<sup>181</sup> tion  $\mathcal{W}(x)$  is to be solved for and depends on the distribution of the parameters  $a, b$ , as  
<sup>182</sup> well as the normal stress distribution at times approaching  $t_{in}$ .

<sup>183</sup> In addition to showing the existence of (10), Ray & Viesca (2017) also determined  
<sup>184</sup> whether these types of solutions would likely represent how slip rate would locally, quasi-  
<sup>185</sup> statically diverge in the moments preceding dynamic rupture in a model with rate- and  
<sup>186</sup> state-dependent friction. Following Viesca (2016a,b), this was done in treating the dis-  
<sup>187</sup> tribution  $\mathcal{W}(x)$  as a fixed point of a dynamical system and assessing its stability. The  
<sup>188</sup> analysis reduces to determining whether perturbations to the diverging slip rate (10) them-  
<sup>189</sup> selves diverge or decay as  $t_f \rightarrow 0$ . We look for perturbations of the form Barenblatt  
<sup>190</sup> (1996)

$$\text{<sup>191</sup> } V(x, t) = \frac{D_c(x)}{t_f} [\mathcal{W}(x) + \omega(x)(t_f/t_o)^{-\lambda}] \quad (11)$$

<sup>193</sup> where the distribution  $\omega(x)$  and constant  $\lambda$  are to be determined and reduce to eigen-  
<sup>194</sup> functions and eigenvalues of an eigenvalue problem Ray & Viesca (2017), respectively,  
<sup>195</sup> and where  $t_o$  is an arbitrary timescale. If a mode exists with  $\text{Re}(\lambda) > 0$ , then the so-  
<sup>196</sup> lution (10) is said to be unstable, and the solution is stable in the absence of such a mode.

### <sup>197</sup> 4 Assessing the influence of fault heterogeneity on earthquake nucle- <sup>198</sup> ation

<sup>199</sup> The stability analysis of solutions (10) is particularly significant when fault fric-  
<sup>200</sup> tional properties are nonuniformly distributed. For a fault with homogeneous proper-  
<sup>201</sup> ties an invariance exists with respect to translations in space and a solution of the type  
<sup>202</sup> (10) could be said to exist about any point on the fault. In contrast, for a fault with het-  
<sup>203</sup> erogeneous properties, there are a finite number of blow-up solutions (10) distributed at

critical points on the fault. Only a subset of these solutions are stable; and, in turn, only those associated critical points on the fault can be expected to nucleate a dynamic rupture Ray & Viesca (2017).

However, an important question remains: how does the rate at which properties vary along the fault affect the existence of solutions (10), as well as their stability? A related question of particular interest is whether, and under what conditions, may frictional properties be effectively homogenized. Rather than considering the variations of parameters  $a$  or  $b$  individually, we focus on variations of the magnitude of steady-state rate-weakening, as well as a measure of its relative magnitude, defined respectively as

$$m(x) = b(x) - a(x)$$

$$r(x) = 1 - a(x)/b(x)$$

We consider simple forms for their along-fault variations on fault

$$m(x) = m_o + m_1 \cos(\kappa x / L_{ef}) \quad (12a)$$

$$r(x) = r_o + r_1 \cos(\kappa x / L_{ef}) \quad (12b)$$

where  $\kappa$  is a dimensionless wavenumber and  $L_{ef}$  is an elasto-frictional length, which is a placeholder for  $L_{nh}$  or  $L_{bh}$ , depending on whether  $b$  varies or not, respectively, in arriving to the distributions (12). The dimensionless wavelength  $\Lambda = 2\pi/\kappa$  measures the lengthscale of property variation against the elasto-frictional length. We now analyze how  $\kappa$  affects the blow-up solutions and their stability.

## 5 Results

We highlight blow-up solutions and their stability results for three particular cases in Fig. 1: a case of homogenously distributed parameters (Fig. 1a), and two heterogeneous cases with an increasing degree of heterogeneity, i.e., an increase in the wavenumber  $\kappa$  (Fig. 1b,c). In the homogeneous case, there is one solution for the distribution  $\mathcal{W}(x)$  (Fig. 1e) that may be spatially translated (Fig. 1d). An analysis of its stability shows that it is a stable, attractive solution. Specifically, there are only two modes with  $\text{Re}(\lambda) \geq 0$ : these are associated spatial and temporal translational invariance (Fig. 1g, dashed and solid lines, respectively) and do not influence solution stability Viesca (2016a). Introducing some heterogeneity (Fig. 1b), spatial translational variance no longer exists, and we find that blow-up solutions are confined to extrema in the distribution (Fig.

1e). In this case the solution at the maximum of  $r$  is stable, at that at the minimum is  
 236 unstable. A stability analysis of the former shows no modes with  $\text{Re}(\lambda) > 0$ , apart from  
 237 the temporal invariance mode (Fig. 1h, solid black curve). A stability analysis of the lat-  
 238 ter shows an unstable mode (Fig. 1i, red curve), in addition to the translational mode  
 239 (Fig. 1i, black curve). Considering a heterogeneous case with increase  $\kappa$  (Fig. 1c), we  
 240 find that the solutions are still confined to extrema (Fig. 1f, in which solutions for only  
 241 two extrema are shown). However, we now find that the stability of the solutions at the  
 242 extrema are reversed from the case of Fig. 1b: the solutions at the maxima are unsta-  
 243 ble and those at minima are stable (Fig. 1j,k). This stability implies that the regions  
 244 with the lowest magnitude of steady-state rate-weakening are now the attractive loca-  
 245 tion for instability.

247 The remarkable reversal of stability with decreasing wavelength of property vari-  
 248 ations is reflected in numerical solutions for the evolution of slip rate (Fig. 2). Begin-  
 249 ning with initially steady-state conditions, we introduce at  $t = 0$  a locally peaked stress-  
 250 ing rate centered at a position between a maximum and minimum in the distribution  
 251 of  $r$ . An unstable acceleration of slip follows and we plot in Fig. 2b the slip rate, scaled  
 252 by its maximum value at snapshots in time. As time progresses, the slip rate diverges  
 253 and approaches the expected distribution of the stable blow-up solution (green dashed  
 254 line, Fig. 2b). In Fig. 2c, we increase  $\kappa$  to the point where the stabiltiy is reversed. This  
 255 reversal is reflected in the evolution of the diverging slip rate (Fig. 2d).

256 To better understand the reversal of stability as  $\kappa$  changes, we examined its influ-  
 257 ence on  $\lambda_{max}$ , defined as the maximum eigenvalue associated with the blow-up solutions  
 258 at the peak and troughs of the distributions (Figs. 3 and 4a). As before, when  $\text{Re}(\lambda_{max}) >$   
 259 0, the blow-up solution is unstable, and stable otherwise. We consider two elementary  
 260 scenarios: both  $r(x)$  and  $m(x)$  vary in phase, as may occur if  $a$  varies and  $b$  is held fixed  
 261 (Fig. 3); or a variable  $m(x)$  under a constant and uniform  $r$  (Fig. 4). In each case, the  
 262 blow-up solutions are found to exist only at critical regions: about the extrema of pa-  
 263 rameter distributions, and, in some cases, between them. In Figs. 3 and 4a, the cyan and  
 264 blue curves are indicator of the stability of the blow-up solutions at the minimum and  
 265 maximum of the parameter variations, respectively. In Fig. 4a, the magenta-colored curve  
 266 corresponds to the stability of the blow-up solutions that occur around the inflection points  
 267 of  $m(x)$  when wavenumber  $\kappa$  is within the red-colored regime. In the following sub-sections,

268 we comment on the behavior at long, intermediate, and short wavelengths of parameter variations.  
 269

270 We make a brief aside to discuss what is meant by long (or short) wavelengths. We  
 271 recall that we have scaled wavelengths and wavenumber by an elasto-frictional length,  
 272 such that, for example, the interpretation of small  $\kappa$  is that wavelengths are large in com-  
 273 parison to this length. However, we also recall that another relevant length exists: the  
 274 nucleation length denoted by  $L$ , which is the half-length of the region for the distribu-  
 275 tion  $\mathcal{W}$  (e.g., illustrated in Figs. 1 and 2). In the homogeneous limit for the cases stud-  
 276 ied here, in which  $a/b = 0.5$ ,  $L$  is comparable to the elasto-frictional length:  $L = \pi L_{bh}$   
 277 Viesca (2016a). Thus, a distinction does not need to be explicitly made in our discus-  
 278 sions above and to follow. However, we must note that, for homogeneous properties, as  
 279  $a/b \rightarrow 1$ ,  $L$  generally diverges in comparison with the elasto-frictional lengthscales used  
 280 here ( $L_b$  or  $L_{bh}$ ) Viesca (2016a,b). In this limit, careful attention must be paid to the  
 281 relevant lengthscale with which to compare distances over which frictional properties vary.  
 282 The most relevant length is  $L$ , the length over which solutions (10) sample property vari-  
 283 ations. While  $L$  is not known a priori for arbitrary property variations,  $L$  is known for  
 284 homogeneous frictional properties [Rubin and Ampuero, 2005; Viesca 2016a,b], which  
 285 provides a first estimate using averaged quantities for heterogeneous faults. Apart from  
 286 the elasto-frictional length scale,  $L$  is dependent on the ratio  $a/b$ . For the half-space and  
 287 thin-slab configurations, respectively,  $L = L_b/[\pi(1 - a/b)^2]$  and  $L = L_{bh}/(1 - a/b)$  in  
 288 the limit  $a/b \rightarrow 1$  Viesca (2016a,b)

## 289 5.1 Long and intermediate wavelengths

290 With variations over long wavelengths ( $\kappa \ll 1$ ), we find that whether the local  
 291 maxima or minima of frictional properties are the locations of attractive blow-up depends  
 292 on what frictional properties vary. In Fig. 3, in which  $m$  and  $r$  both vary in phase, blow-  
 293 up solutions about the local maxima are stable and those about the minima are unsta-  
 294 ble (as in Fig. 2a,b). To contrast, in Fig. 4a, we find that under fixed  $r$  and variable  $m$ ,  
 295 it is the minima of  $m$  that are attractive locations for instability.

296 At small values of  $\kappa$ , we also find a third possibility for instability progression when  
 297  $r$  is fixed and  $m$  varies: blow-up of slip rate at a region between the maximum and min-  
 298 imum. As alluded to above, this third possibility occurs transiently as  $\kappa$  increases: first

299 appearing close to  $\kappa = 0.2$  and disappearing close to  $\kappa = 0.35$  (red areas in Fig. 4).  
 300 Its corresponding value of  $\lambda_{max}$  is shown in magenta in Fig. 4a. The appearance of these  
 301 intervening solutions coincides with the loss of stability of blow-up solutions occurring  
 302 about the minima of  $m$ , and their disappearance coincides with the return of stability  
 303 of the solutions occurring about the maxima. In Fig. 4b we illustrate the abrupt appear-  
 304 ance of these intervening blow-up solutions. At  $\kappa = 0.15$  we show the solution for  $\mathcal{W}(x)$   
 305 that occurs about a maximum. Additional solutions for  $\mathcal{W}(x)$  suddenly appear in the  
 306 region between the maximum and adjacent minima around  $\kappa = 0.2$  and are stable. As  
 307  $\kappa$  increases further, the position of these attractive intervening solutions approaches the  
 308 solution at the maximum. Ultimately, the intervening solutions collide with that at the  
 309 maximum around  $\kappa = 0.35$ . At this point, the latter solution remains and regains sta-  
 310 bility.

311 Intermediate values of kappa mark a qualitative transition in stability behavior of  
 312 the blow-up solutions. As  $\kappa$  increases from small values,  $\lambda_{max}$  takes on its most positive  
 313 and negative values close to  $\kappa = 1$  for the two cases. Subsequently, an exchange of sta-  
 314 bility of the solutions at the maxima and minima occurs. It is this exchange of stabil-  
 315 ity that is captured in Fig 2. This exchange of stability repeats indefinitely as  $\kappa$  increases.

316 In Fig. 3 we show the value of the nucleation half-length  $L$  for solutions at both  
 317 extrema (dashed and dash-dotted lines).  $L$  is shown as a relative change from its value  
 318 under homogeneous frictional properties ( $\kappa = 0$ ), for which  $L = \pi L_{bh}$  Viesca (2016a).  
 319 At long wavelengths, there is a small departure from the homogeneous value, which matches  
 320 the asymptotic behavior of  $\lambda_{max}$ . The departure remains modest (<20%) at interme-  
 321 diate wavelengths, and returns to zero precisely when the exchange of stability occurs.

## 322 5.2 Short wavelengths and homogenization

323 Remarkably, the behavior at large  $\kappa$ , at which the frictional properties are highly  
 324 heterogeneous, is that of a homogeneous fault with the spatially averaged values of the  
 325 variable properties. Specifically, the blow-up solutions at the extrema converge to the  
 326 spatially translatable solution under homogeneous conditions for the average value of  $a/b =$   
 327 0.4. As  $\kappa \rightarrow \infty$ ,  $\mathcal{W}(x)$  at both the maxima and minima converge towards the homo-  
 328 geneous solution, in which  $L = \pi L_{bh}$  and, to within a spatial translation,  $\mathcal{W}(x) = [1 +$   
 329  $\cos(x/L_{bh})]/2$ , where  $L = \pi L_{bh}$  Viesca (2016a). Simultaneously in this limit,  $\lambda_{max}$  and

330 the corresponding eigenmode  $\omega(x)$  asymptotically approach the expected values for a trans-  
 331 lational symmetry mode:  $\lambda = 0$  and  $\omega(x) = \mathcal{W}'(x) = -\sin(x/L_{bh})$  Viesca (2016a).  
 332 That a translational invariance re-emerges is the consequence of the maxima and min-  
 333 ima being separated over distances much smaller than the nucleation length  $L$  as  $\kappa \rightarrow$   
 334  $\infty$ . The convergence of  $L$  and  $\lambda_{max}$  for the case of variable  $r$  and  $m$  is shown in Fig. 3,  
 335 and the convergence of  $\lambda_{max}$  for the case of fixed  $r$  and variable  $m$  is shown in 4. Dur-  
 336 ing the convergence, there is an exchange of stability between the solutions at maxima  
 337 and minima, with an ever-decreasing amplitude for the eigenvalue  $\lambda_{max}$  for each solu-  
 338 tion. For the case of variable  $r$  and  $m$ , the stability exchange occurs at integer values  
 339 of  $\kappa$  [Supplementary Materials].

## 340 6 Conclusion

341 We show that homogenization of frictional parameters for slip rate- and state-dependent  
 342 friction is justifiable in the limits of variations occurring over relatively long or short length-  
 343 scales. In the former case, frictional parameters vary gradually relative to spatial vari-  
 344 tions in slip rate, which scale with the elasto-frictional length. The evolution of slip rate  
 345 is expected to follow that of a homogeneous fault with the local, zeroth-order approx-  
 346 imation of the variable parameters. In the latter case, the behavior is that of a homo-  
 347 geneous fault with properties being an average over the elasto-frictional length, which  
 348 samples the rapid variations in this short-wavelength limit.

349 How does one determine if the property variations of a fault lie within either end-  
 350 member regime, or an intermediate one? If a length scale for variation is posited, or oth-  
 351 erwise assumed to exist on some basis, it must then be first compared with an elasto-  
 352 frictional length. For a fault well represented as slip between elastic half-spaces, we re-  
 353 call that the appropriate length scale is  $L_b = \mu D_c / (\sigma b)$ . For  $D_c$  at the mm-scale im-  
 354 plies an elasto-frictional length of the order of 10-100 m for shear modulus, normal stress,  
 355 and coefficient  $b$  of the orders of 10 GPa, 10-100 MPa, and 0.01, respectively. Values of  
 356  $D_c$  more typically found in laboratory-scale experiments, on the order of 10-100  $\mu\text{m}$  would  
 357 decrease that estimate by up to two orders of magnitude. For pore-fluid pressure approach-  
 358 ing lithostatic, the reduction of the effective normal stress  $\sigma$  to very low values may in-  
 359 flate the estimates of the elasto-frictional length, easily placing a fault in the short-wavelength  
 360 regime.

361 **Acknowledgments**

362 The authors gratefully acknowledge support from NSF via grants EAR-1344993  
 363 and EAR-1653382 and from the Southern California Earthquake Center (SCEC). SCEC  
 364 is funded by NSF Cooperative Agreement EAR-1600087 and USGS Cooperative Agree-  
 365 ment G17AC00047.

366 **References**

- 367 Aldam, M., Weikamp, M., Spatschek, R., Brener, E. A., & Bouchbinder, E. (2017).  
 368 Critical Nucleation Length for Accelerating Frictional Slip. *Geophys. Res. Lett.*,  
 369 44(22), 11,390–11,398. doi: <https://doi.org/10.1002/2017GL074939>
- 370 Ampuero, J.-P., Ripperger, J., & Mai, P. M. (2006). Properties of dynamic earth-  
 371 quake ruptures with heterogeneous stress drop. In A. McGarr, R. E. Abercrombie,  
 372 H. Kanamori, & G. Di Toro (Eds.), *Radiated energy and the physics of earth-*  
 373 *quakes* (pp. 255–261). Washington, D. C.: Geophysical Monograph Series 170,  
 374 American Geophysical Union. doi: <https://doi.org/10.1029/170GM25>
- 375 Aochi, H., & Ide, S. (2004). Numerical study on multi-scaling earthquake rupture.  
 376 *Geophysical Research Letters*, 31(2). doi: <https://doi.org/10.1029/2003GL018708>
- 377 Barenblatt, G. I. (1996). *Scaling, self-similarity, and intermediate asymptotics: di-*  
 378 *mensional analysis and intermediate asymptotics* (Vol. 14). Cambridge University  
 379 Press. doi: <https://doi.org/10.1017/CBO9781107050242>
- 380 Bar-Sinai, Y., Brener, E. A., & Bouchbinder, E. (2012). Slow rupture of frictional in-  
 381 terfaces. *Geophys. Res. Lett.*, 39(3). doi: <https://doi.org/10.1029/2011GL050554>
- 382 Bayart, E., Svetlizky, I., & Fineberg, J. (2015). Fracture mechanics determine the  
 383 lengths of interface ruptures that mediate frictional motion. *Nat. Phys.*, 1–6. doi:  
 384 <https://doi.org/10.1038/nphys3539>
- 385 Bilby, B., & Eshelby, J. (1968). Fracture, an advanced treatise. In *Microscopic and*  
 386 *macroscopic fundamentals* (Vol. 1, p. 29). Academic Press New York and London.
- 387 Blanpied, M. L., Lockner, D. A., & Byerlee, J. D. (1991). Fault stability inferred  
 388 from granite sliding experiments at hydrothermal conditions. *Geophys. Res. Lett.*,  
 389 18(4), 609–612. doi: <https://doi.org/10.1029/91GL00469>
- 390 Dieterich, J. H. (1978). Time-dependent friction and the mechanics of stick-slip.  
 391 *Pure Appl. Geophys.*, 116(4), 790–806. doi: <https://doi.org/10.1007/BF00876539>

- 392 Dieterich, J. H. (1981). Constitutive properties of faults with simulated gouge. *Mechanical behavior of crustal rocks: the Handin volume*, 24, 103–120. doi: <https://doi.org/10.1029/GL008i007p00653>
- 393  
394
- 395 Dieterich, J. H. (1992). Earthquake nucleation on faults with rate-and state-  
396 dependent strength. *Tectonophysics*, 211(1), 115–134. doi: [https://doi.org/10.1016/0040-1951\(92\)90055-B](https://doi.org/10.1016/0040-1951(92)90055-B)
- 397  
398 Dublanchet, P. (2017, 10). The dynamics of earthquake precursors controlled by ef-  
399 fective friction. *Geophysical Journal International*, 212(2), 853–871. doi: 10.1093/  
400 gji/ggx438
- 401 Goldsby, D. L., & Tullis, T. E. (2011). Flash Heating Leads to Low Frictional  
402 Strength of Crustal Rocks at Earthquake Slip Rates. *Science*, 334(6053), 216–218.  
403 doi: 10.1126/science.1207902
- 404 Ide, S., & Aochi, H. (2005a). Earthquakes as multiscale dynamic ruptures with het-  
405 erogeneous fracture surface energy. *Journal of Geophysical Research: Solid Earth*,  
406 110(B11).
- 407 Ide, S., & Aochi, H. (2005b). Earthquakes as multiscale dynamic ruptures with het-  
408 erogeneous fracture surface energy. *J. Geophys. Res.*, 110(B11), 3575–10. doi:  
409 <https://doi.org/10.1029/2004JB003591>
- 410 Kammer, D. S., Radiguet, M., Ampuero, J.-P., & Molinari, J.-F. (2015). Linear  
411 Elastic Fracture Mechanics Predicts the Propagation Distance of Frictional Slip.  
412 *Tribology Letters*, 57(3). doi: <https://doi.org/10.1007/s11249-014-0451-8>
- 413 Ke, C. Y., McLaskey, G. C., & Kammer, D. S. (2018). Rupture Termination in  
414 Laboratory-Generated Earthquakes. *Geophys. Res. Lett.*, 308, 681–9. doi: <https://doi.org/10.1029/2018GL080492>
- 415  
416 Lipovsky, B. P., & Dunham, E. M. (2017). Slow-slip events on the Whillans Ice  
417 Plain, Antarctica, described using rate-and-state friction as an ice stream slid-  
418 ing law. *J. Geophys. Res. Earth Surf.*, 122(4), 973–1003. doi: <https://doi.org/10.1002/2016JF004183>
- 419  
420 Puzrin, A. M., & Germanovich, L. N. (2005). The growth of shear bands in the  
421 catastrophic failure of soils. *P. Roy. Soc. A.*, 461(2056), 1199–1228. doi: <https://doi.org/10.1098/rspa.2004.1378>
- 422  
423 Ray, S., & Viesca, R. C. (2017). Earthquake Nucleation on Faults With Heteroge-  
424 neous Frictional Properties, Normal Stress. *J. Geophys. Res.*, 122(10), 8214–8240.

- 425 doi: <https://doi.org/10.1002/2017JB014521>
- 426 Rice, J. R. (1968). A path independent integral and the approximate analysis of  
427 strain concentration by notches and cracks. *Journal of applied mechanics*, 35(2),  
428 379–386.
- 429 Rice, J. R. (2006). Heating and weakening of faults during earthquake slip. *J. Geo-*  
430 *phys. Res.*, 111, B05311. doi: <https://doi.org/10.1029/2005JB004006>
- 431 Rice, J. R., Lapusta, N., & Ranjith, K. (2001). Rate and state dependent friction  
432 and the stability of sliding between elastically deformable solids. *J. Mech Phys.*  
433 *Solids*, 49(9), 1865–1898. doi: [https://doi.org/10.1016/S0022-5096\(01\)00042-4](https://doi.org/10.1016/S0022-5096(01)00042-4)
- 434 Rice, J. R., & Ruina, A. L. (1983). Stability of steady frictional slipping. *J. Appl.*  
435 *Mech.*, 50, 343–349. doi: <https://doi.org/10.1115/1.3167042>
- 436 Ripperger, J., Ampuero, J.-P., Mai, P. M., & Giardini, D. (2007). Earthquake source  
437 characteristics from dynamic rupture with constrained stochastic fault stress. *J.*  
438 *Geophys. Res.*, 112(B4). doi: <https://doi.org/10.1029/2006JB004515>
- 439 Rubin, A. M., & Ampuero, J.-P. (2005). Earthquake nucleation on (aging) rate  
440 and state faults. *J. Geophys. Res.*, 110, B11312. doi: <https://doi.org/10.1029/2005JB003686>
- 441 Rubin, A. M., Gillard, D., & Got, J. L. (1999). Streaks of microearthquakes along  
442 creeping faults. *Nature*, 400(6745), 635–641. doi: <https://doi.org/10.1038/23196>
- 443 Ruina, A. (1983). Slip instability and state variable friction laws. *J. Geophys. Res.*,  
444 88(B12), 10359–10370. doi: <https://doi.org/10.1029/JB088iB12p10359>
- 445 Stesky, R. M. (1975). *The mechanical behavior of faulted rock at high tempera-*  
446 *ture and pressure*. (Unpublished doctoral dissertation). Massachusetts Institute of  
447 Technology.
- 448 Tse, S. T., & Rice, J. R. (1986). Crustal Earthquake Instability in Relation to the  
449 Depth Variation of Frictional Slip Properties. *J. Geophys. Res.*, 91, 9452–9472.  
450 doi: <https://doi.org/10.1029/JB091iB09p09452>
- 451 Viesca, R. C. (2016a). Self-similar slip instability on interfaces with rate- and state-  
452 dependent friction. *Proceedings of the Royal Society A: Mathematical, Physical*  
453 *and Engineering Science*, 472(2192), 20160254. doi: <https://doi.org/10.1098/rspa.2016.0254>
- 454 Viesca, R. C. (2016b). Stable and unstable development of an interfacial sliding in-  
455 stability. *Phys. Rev. E*, 93(6), 060202(R). doi: <https://doi.org/10.1103/PhysRevE.93.060202>

458 .93.060202

459 Waldhauser, F., Ellsworth, W. L., Schaff, D. P., & Cole, A. (2004). Streaks, multi-  
460 plets, and holes: High-resolution spatio-temporal behavior of Parkfield seismicity.  
461 *Geophys. Res. Lett.*, 31(18), 619–5. doi: <https://doi.org/10.1029/2004GL020649>

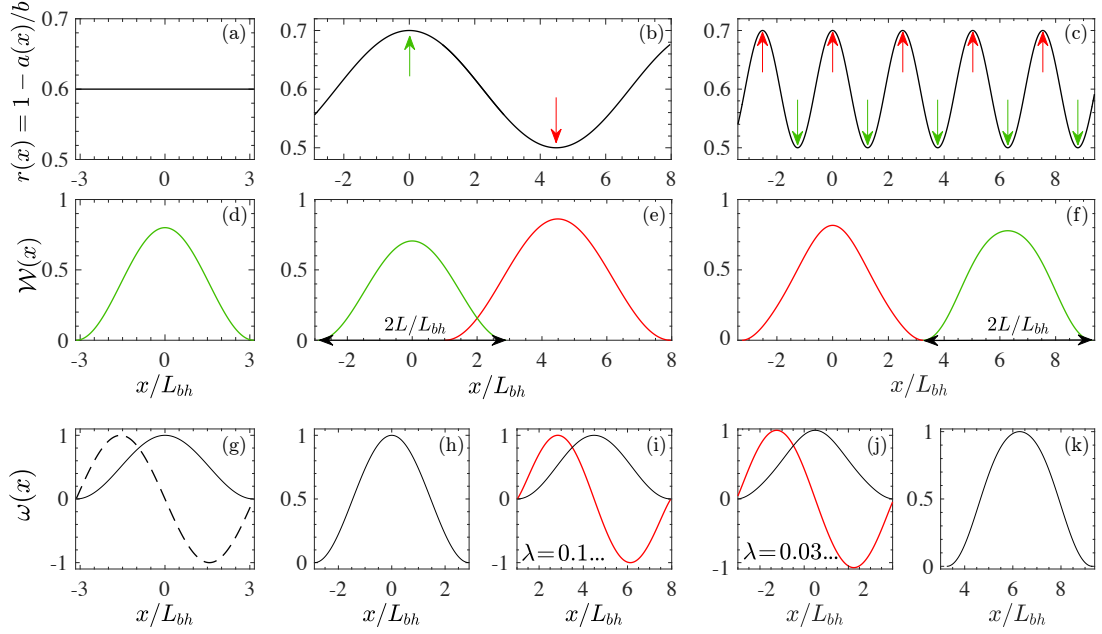


**Figure 1.** Fixed point solutions and their stability under different wavelengths of frictional property variation. Plots, along the fault length  $x$ , of (a–c) the variation of  $r = 1 - a/b$ ; (d–f) stable (green) and unstable (red) blow-up solutions (10) corresponding to the overlying distributions; and (g–k) eigenmodes including temporal (black) and spatial (dashed) symmetry modes, and unstable modes (red) with  $\text{Re}(\lambda) > 0$ . Panels in rows (d–f) and (g–k) correspond to the property variations (a–c) at the top of the panel columns. Introduction of heterogeneity restricts blow-up solutions to frictional property extrema. Only a subset of these solutions are stable and increasing the degree of heterogeneity leads to reversals in stability.

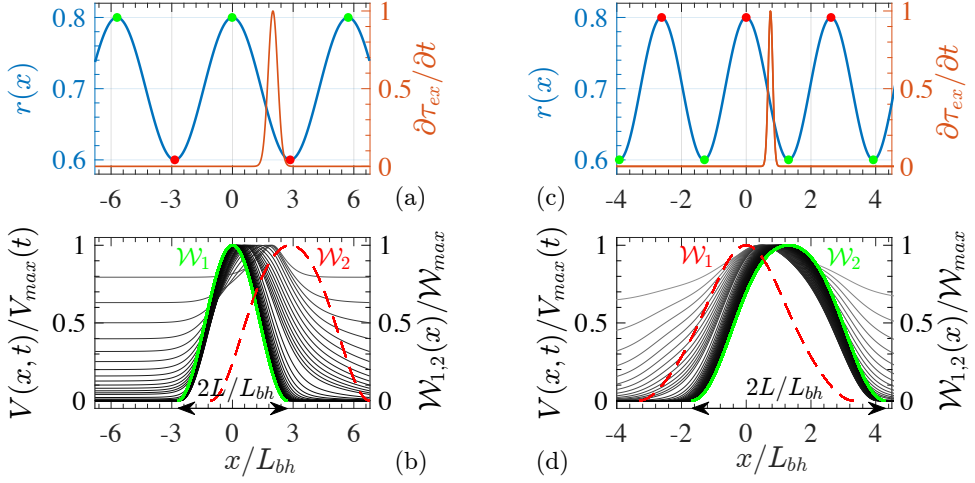


**Figure 2.** Decreasing the wavelength of frictional property variations leads to a reversal in which fault locations are attractive for instability development. (a,c) Distributions  $r(x) = 1 - a(x)/b$  along fault position  $x$  (blue) with two different wavelengths and location of a local, constant stressing rate (red). Green (red) dots highlight locations of stable (unstable) blow-up solutions. (b,d) Numerical solutions for slip rate evolution for a fault subject to the local stressing for distributions (a) and (c), respectively. Slip rate shown at instants in time, scaled by the maximum value at each time (greyscale) and blow-up solutions scaled by peak values (red, green). Green and red curves correspond to stable and unstable solutions.

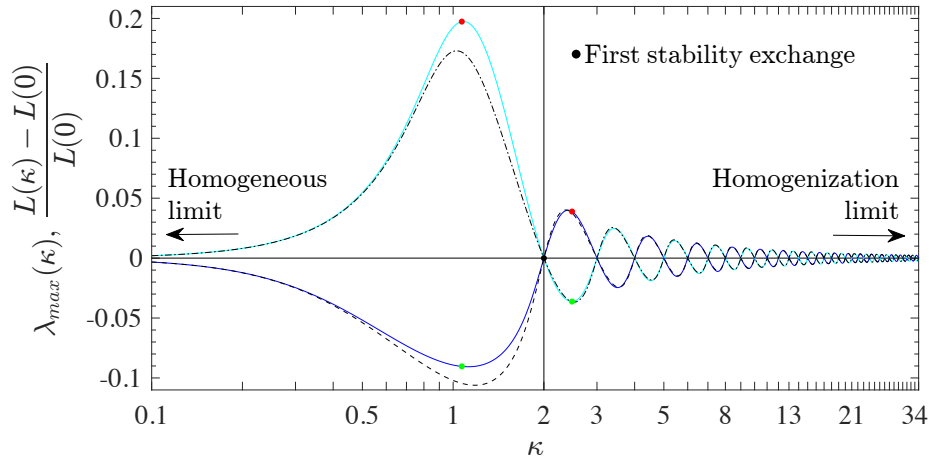


**Figure 3.** Exchange of stability of blow-up solutions occurring about the maxima and minima of a distribution of a frictional property distribution. The absolute  $m$  and relative rate weakening  $r$  vary in phase with  $r(x) = 0.6 + 0.1 \cos(\kappa x/L_{bh})$ , similarly to Fig. 2. We solve for the stability of blow-up solutions as a function of the wavenumber  $\kappa$ . We show the maximum eigenvalue  $\lambda_{max}$  for blow-up solutions occurring about the maxima (blue) and minima (cyan) of the distribution of  $r$ . Solutions are unstable if  $\lambda_{max} > 0$  and stable otherwise. Colored dots correspond to cases examined in Fig. 2. Stability exchanges occur at integer values of  $\kappa$ . Also shown are the corresponding values for the nucleation half-length  $L$  for blow-up solutions at maxima (dashed) and minima (dash-dotted), relative to its value in the homogeneous limit  $L(\kappa = 0) = \pi L_{bh}$ .

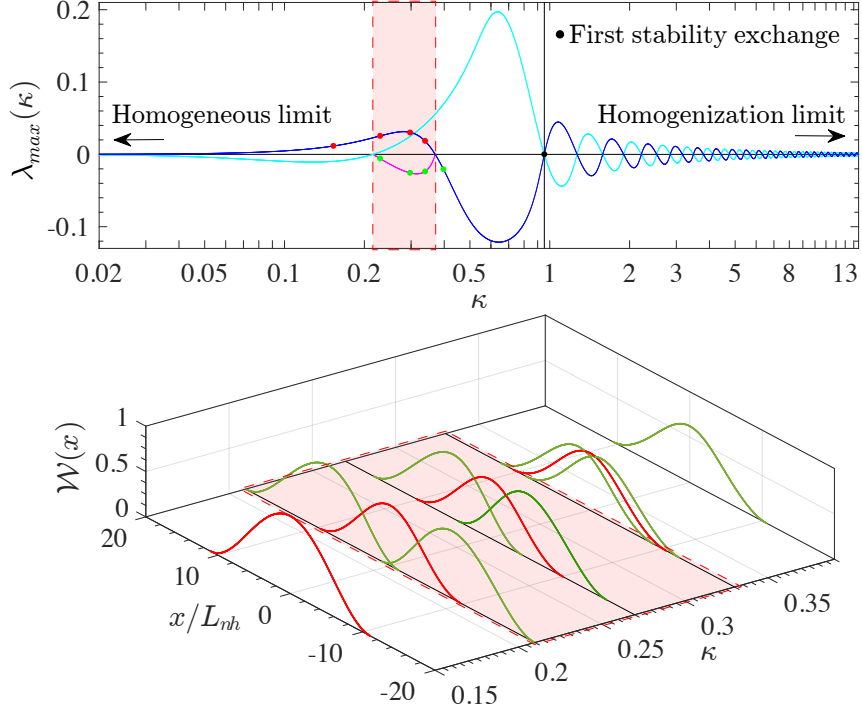


**Figure 4.** Under fixed  $r = 1 - a/b$  and variable  $m = b - a$ , an exchange of stability occurs similarly to that in Fig. 3, except with additional bifurcations at small values of  $\kappa$  (red region). Here  $m(x) = 0.06 + 0.02 \cos(\kappa x / L_{nh})$  with a constant  $r = 0.6$ . (a) Plot of the maximum eigenvalue  $\lambda_{max}$  as a function  $\kappa$  from the stability analysis of blow-up solutions at maxima (blue) and minima (cyan).  $\lambda_{max}$  for a third type of blow-up solution, which appears in the region between extrema, is shown in magenta. (b) Illustration of the sudden appearance and disappearance of the third-type of blow-up solution (see text for description). The green and red dots in (a) correspond to the solutions of the same colors in (b); these colors correspond to stable (attractive) or unstable (unattractive) blow-up solutions.